Secondary Metal-Ligand Interactions Supported Copper(I) Emitters for High-Efficiency OLEDs

Ao Ying, Yao Tan, Shaolong Gong *

Department of Chemistry, Hubei Key Lab on Organic and Polymeric Optoelectronic Materials, Wuhan University, Wuhan 430072, China
E-mail: slgong@whu.edu.cn

Abstract: The most prominent way of tuning optoelectronic properties of copper(I) emitters is primary-sphere ligand engineering, but little attention has been placed on noncovalent interactions. Here we demonstrate an effective strategy to introduce secondary metal-ligand interactions into two-coordinate Cu(I) emitters with the goals of optimizing conformation dynamics and improving optical properties. As a proof of concept, a panel of Cu(I) complexes are developed *via* chalcogen-heterocyclic engineering on the 1,2-positions of carbazole ligand. These complexes have distinct noncovalent metal-ligand interactions mainly originating from chalcogen···Cu and Cu···chalcogen−C orbital interactions, verified by single-crystal structure and theoretical simulation. Thanks to confined conformations and reduced ligand-ligand rotation freedom, the optimized Cu(I) emitters afford high emission quantum yields of up to 93% together with large radiative rate constants of up to 1.2 $\times 10^6$ s^{-1}. This work unlocks the large potential of noncovalent interactions in developing excellent Cu(I) emitters for cost-effective and high-efficiency OLEDs.

Keywords: Copper(I) Emitter, Secondary Metal-Ligand Interaction, Organic Light-Emitting Diode (OLED), Carbene-Metal-Amide (CMA), Thermally Activated Delayed Fluorescence (TADF)

Introduction

Noncovalent interactions such as hydrogen, chalcogen, halogen, and pnictogen bonds, as well as π···π interactions have attached paramount attentions for promising capability of tailoring optoelectronic properties of organic semiconductors, such as charge carrier mobility, energy level, absorption, and emission.[1] Therefore, understanding and control of noncovalent interactions in organic semiconductors is paramount for applications within the fields of organic photovoltaics,[2] organic field effect transistors,[3] and organic light-emitting diodes (OLEDs).[4] So far, various noncovalent interactions have been utilized to construct emissive materials. To illustrate, hydrogen bonding and π···π interactions have been widely reported to play an important role in determining emissive properties of thermally activated delayed fluorescence (TADF) and room temperature phosphorescence materials.[5] For organometallic complexes, noncovalent interactions have also been widely explored in the control of secondary coordination sphere and self-assembly processes.[6] Due to unique ability of tuning various coordination spheres and geometries, secondary metal-ligand interactions have been well exploited as spontaneous force to arrange building blocks for supramolecular polymers, organometallic clusters or aggregates.[7] However, the influence of secondary metal-ligand interactions on the photophysical properties of luminescent organometallic complexes, especially for mononuclear organometallic emitters, have been rarely explored and rather understood.

Owing to high abundance, low cost, and the absence of low-lying metal-centered states, mononuclear copper(I) emitters have long been regarded as appealing

replacement for the widely studied iridium(III) and platinum(II) phosphors in OLEDs.[8] Despite extensive efforts in Cu(I) emitters over the past 50 years,[9] achieving comparable performance with noble metal phosphors is still a challenging task. Currently, only a handful of Cu(I) emitters exhibit promising electroluminescent performance with over 20% external quantum efficiencies (EQEs).[10] The mainstream design of Cu(I) emitters is to engineer primary ligands. For instance, early-stage four-coordinate Cu(I) complexes usually phosphoresce from metal-to-ligand charge transfer (MLCT) excited states (**Figure 1**).[11] With the introduction of halogen atoms, three-coordinate Cu(I) complexes have been reported to emit delayed fluorescence from the combined MLCT and halide-to-ligand charge transfer (XLCT) states (**Figure 1**).[10a,b] Similarly, the employment of strong π-donating amide ligands (e.g. carbazole derivates) imparts three-coordinate Cu(I) complexes with distinct TADF properties stemming from ligand-to-ligand charge transfer (LLCT) excited states.[12] Notably, the groundbreaking discovery recently reported by Di and Thompson and co-workers inspire a resurgent interest in the development of coinage metal complexes, especially for two-coordinate Cu(I) emitters.[13] The combination of π-accepting carbene ligands and π-donating amide ligands have been highlighted to construct efficient two-coordinate Cu(I) emitters. With the unique carbene-metal-amide (CMA) motif, this class of Cu(I) complexes not only emit TADF from LLCT excited states, but also deliver high radiative rate constants (k_rs) and promising device performance (the reported highest EQE of 23.6%) (**Figure 1**).[14] Alongside the manipulation of electronic structure, the control of conformation dynamics also plays an important role in

determining optoelectronic properties of Cu(I) CMA emitters.[14b,d,15] The introduction of bulky units into the primary carbene and/or amide ligands is the most straightforward method to limit conformation deformation in excited states. Beyond this, we conceive that the use of secondary metal-ligand interactions may be an alternative approach of tuning the conformation dynamics of Cu(I) CMA emitters.

Chalcogen (Ch) heterocycles have been widely applied in coordination chemistry field because their distinct electronic properties can support versatile secondary metal-ligand interactions.[16] In this study, we developed a class of Cu(I) emitters, Cu-12F, Cu-12T, Cu-12BF, and Cu-12BT, using Ch-heterocycle-fused carbazole derivatives, 10*H*-furo[2,3-a]carbazole (12-F), 10*H*-thieno[2,3-a]carbazole (12-T), 12*H*-benzofuro[2,3-a]carbazole (12-BF) and 12*H*-benzo[4,5]thieno[2,3-a]carbazole (12-BT), as donor ligands in the CMA motif. Similar with typical TADF complexes, the exciton energies and lifetimes of these Cu(I) complexes are mainly influenced by the electronic properties of primary-sphere ligands. Intriguingly, this series of complexes had specific secondary metal-ligand interactions between the central copper and Ch-heterocycle subunits, which significantly affect conformation dynamics. Accordingly, the strong secondary metal-ligand interactions limited conformation deformation in excited states of the S-embedded complexes (Cu-12T and Cu-12BT). In combination with the steric hindrance effect, the panel of complexes exhibited superior Φ_{PLS} of up to 93% together with large k_rs of up to 1.2 $\times 10^6$ s^{-1}.

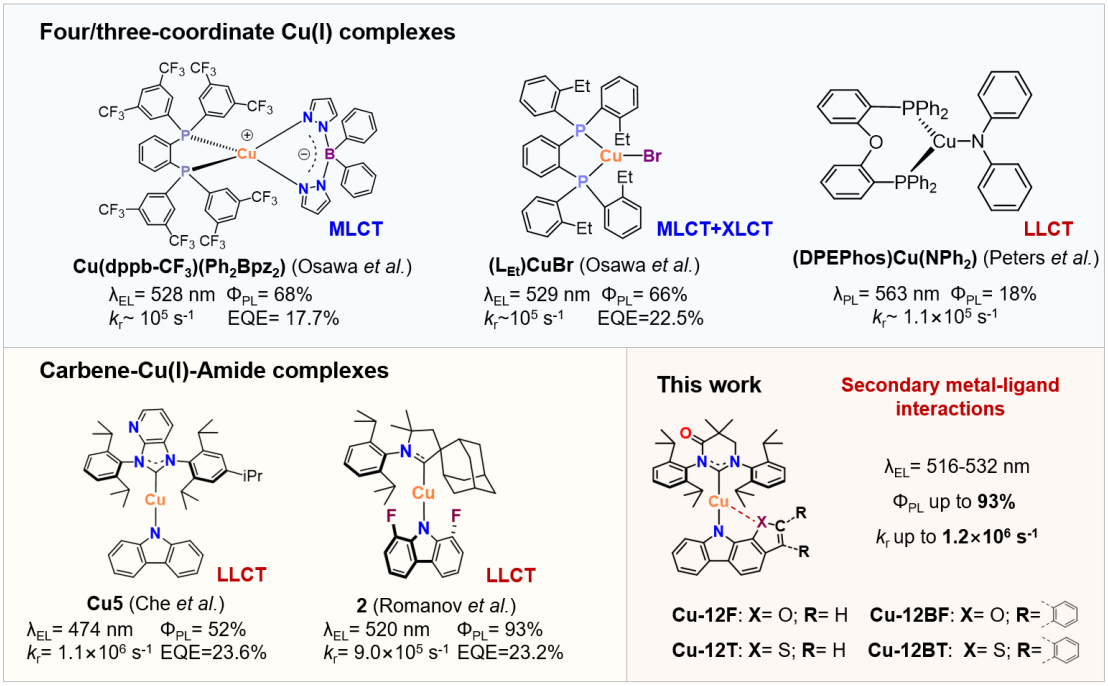

Figure 1. Chemical structures, optical properties, and device performances of Cu(I) emitters reported in literatures and this work.

Results and Discussion

Synthesis and Characterization

The Ch-heterocycle-fused carbazole ligands were prepared by Pd-catalyzed intramolecular cyclization reactions according to the literatures.[17] All the Cu(I) complexes were synthesized *via* simple nucleophilic reactions between the key intermediate of MAC*CuCl and respective carbazole ligands with K_2CO_3 as the base. $^1H/^{13}C$ nuclear magnetic resonance spectroscopy and high-resolution mass spectrometry were conducted to characterize chemical structures of the Cu(I) complexes. Notably, the resonances of ^{13}C-(carbene carbon) followed the order of Cu-12BF (211.0 ppm) > Cu-12F (210.4 ppm) > Cu-12BT (210.3 ppm) > Cu-12T (210.0 ppm). This trend manifests the reduced magnetic shielding around the $C_{carbene}$ of Cu-12F and Cu-12BF, implying the weaker CT transition between the carbene and O-

heterocycle-fused carbazole ligands (12F and 12BF). The electrochemistry study disclosed that all the complexes underwent donor-ligand-attributed irreversible oxidation processes (**Figure S1**). According to the half-wave potentials (calibrated versus ferrocenium/ferrocene), the highest occupied molecular orbital (HOMO) levels of these complexes gradually lifted in the order of Cu-12BF (−5.52 eV) < Cu-12F (−5.49 eV) < Cu-12BT (−5.43 eV) < Cu-12T (−5.38 eV). This is in accordance with the calculated HOMO tendency of the donor ligands (**Figure S2**), largely depending on donor strength of the Ch-heterocycle-fused carbazole ligands (**Figure S3**). Due to the much lower electronegativity and more involvement of S atom in the conjugation, S-heterocycle-fused carbazoles have stronger donor strength than the respective O-heterocycle-fused ones. The introduction of additional fused phenyl moiety can slightly reduce the donor strength of Ch-heterocycle-fused carbazole ligands. Combined with optical band gaps, the lowest unoccupied molecular orbital (LUMO) levels of these complexes were determined to be in the range of −2.85 to −2.88 eV.

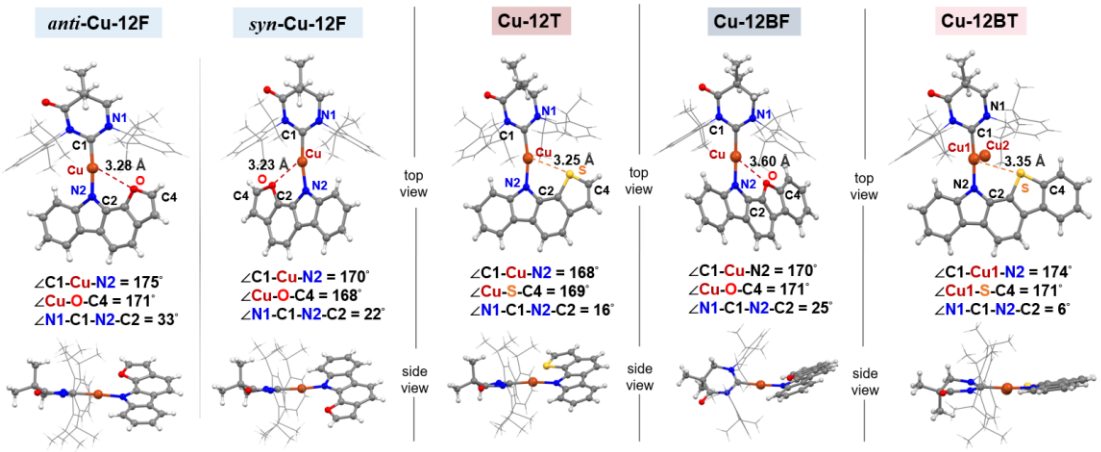

Figure 2. Single-crystal structures of Cu-12F, Cu-12T, Cu-12BF, and Cu-12BT.

The molecular conformations were further confirmed by X-ray crystallographic analysis (**Table S1**). Albeit similar in most bond lengths and bond angles with typical CMA complexes bearing unsubstituted carbazole ligand,[18] this panel of complexes took distinct molecular conformations (**Figure 2**). In terms of ligand-ligand torsion, the O-embedded complexes (Cu-12F and Cu-12BF) had significantly twisted conformations accompanied with large ligand-ligand dihedral angles of up to 33° (**Figure 2**), while the S-embedded complexes (Cu-12T and Cu-12BT) took nearly coplanar geometries. Inspiringly, both *anti*- and *syn*-conformers existed in the crystal of Cu-12F (**Figure 2a**), indicative of large ligand-ligand rotation freedom for Cu-12F. Basically, these complexes possessed nonlinear C-Cu-N configuration with bent ∠C-Cu-N angles of 9-12°. Impressively, the C-Cu and Cu-N bonds of all these complexes significantly oriented to the Ch-heterocycle subunits. Meanwhile, ∠Cu-O-C4 and ∠Cu-S-C4 angles approached about 170°, in favor of electronic coupling between the central copper and O−C/S−C bond. Furthermore, the distances between the copper and chalcogen atoms ranged from 3.23 to 3.60 Å, smaller than the sum of van der Waals radii of Cu and chalcogen atoms. These results clearly established the existence of noncovalent metal-ligand interactions in these complexes.

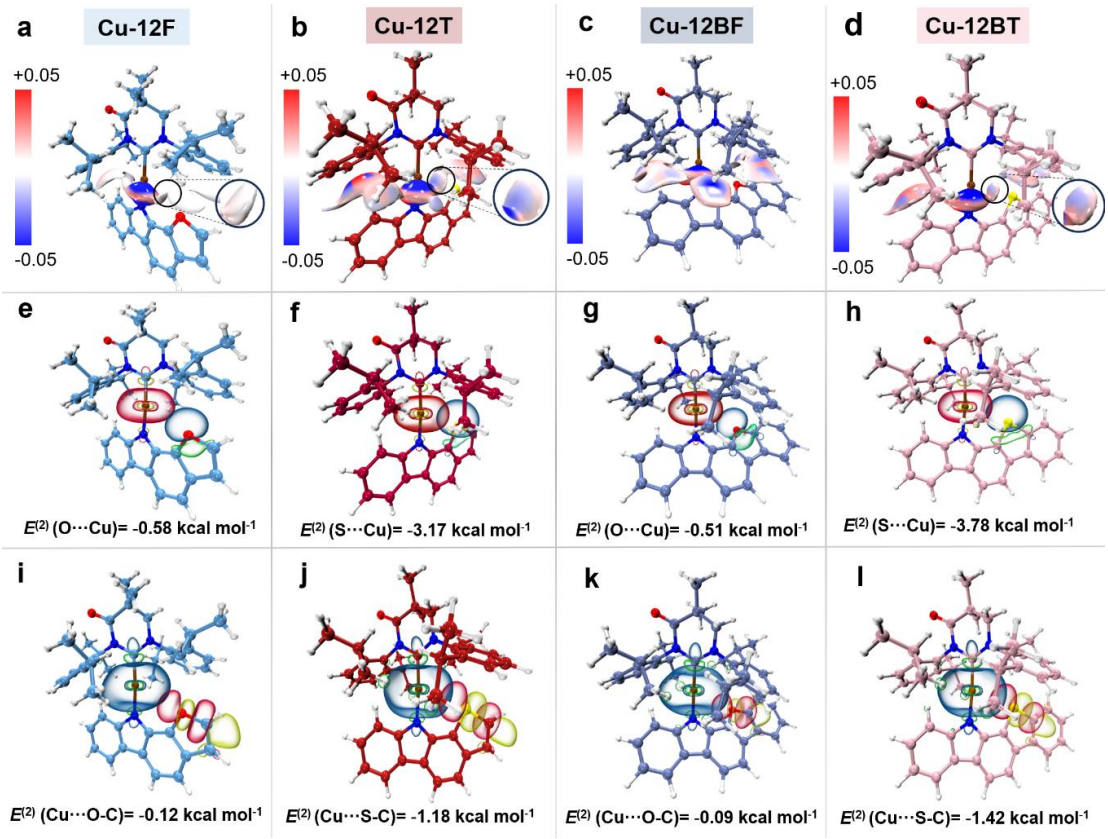

Figure 3. Noncovalent intramolecular interactions of (a) Cu-12F, (b) Cu-12T, (c) Cu-12BF, and (d) Cu-12BT depicted by independent gradient model [Isovalue = 0.005 (electrons/bohr^3)$^{1/2}$]. Attractive and repulsive interactions are colored with blue and red, respectively. Natural bond orbital overlap between the *n*-orbital of chalcogen atoms and the *s*-orbital of copper nucleus in (e) Cu-12F, (f) Cu-12T, (g) Cu-12BF, and (h) Cu-12BT [Isovalue = 0.05 (electrons/bohr^3)$^{1/2}$]. Natural bond orbital overlap between the d-orbital of copper nucleus and σ*-orbital of O−C/S−C bond in (i) Cu-12F, (j) Cu-12T, (k) Cu-12BF, and (l) Cu-12BT [Isovalue = 0.03 (electrons/bohr^3)$^{1/2}$]. $E^{(2)}$ represents stabilization energy taken from the corresponding interactions.

Nature of secondary metal-ligand interactions

To unravel the intrinsic nature of secondary metal-ligand interactions, we firstly conducted noncovalent interaction analysis based on independent gradient model (**Figure 3a-d**).[19] Attractive noncovalent interactions were observed in the region between Cu and S atoms for the S-embedded complexes (**Figure 3b** and **3d**). Whereas, noncovalent interactions were much weaker for Cu-12F and even unobserved for Cu-

12BF (**Figure 3a** and **3c**). Subsequently, we performed natural bond orbital analysis to obtain the secondary perturbation stabilization energy ($E^{(2)}$) between the respective molecular orbitals.[20] For the S-embedded complexes, strong S···Cu orbital interactions were found between the *n*-orbital (lone pair *p*-electrons) of S atom and the valence orbital of Cu atom (mainly contributed by 4*s*-orbital), together with significant $E^{(2)}$ of −3.17 and −3.78 kcal mol^{-1} for Cu-12T and Cu-12BT, respectively (**Figure 3f** and **3h**). However, the O···Cu orbital interactions in Cu-12F and Cu-12BF were much weaker with $E^{(2)}$ values of > −0.6 kcal mol^{-1} (**Figure 3e** and **3g**). Furthermore, the electrons in valence orbital of Cu atoms also interacted with the antibonding σ*(Ch−C) orbitals to afford Cu···Ch−C interactions (**Figure 3e-3h)**. Similar with the Ch···Cu interactions, Cu···Ch−C interactions in the S-embedded complexes were much stronger than that in the O-embedded complexes. This could be attributed to the different orbital components of σ*(Ch−C) orbitals. As displayed in **Table S2**, the antibonding orbitals of S atoms are dominated by *p* orbitals (> 80% orbital parentage) when forming σ*(S−C) orbitals, therefore extending interaction regions to enlarge the orbital overlaps. Additionally, Cu-12F, Cu-12T, and Cu-12BT had tiny electrostatic interaction energies (**Figure S4** and **Table S3)**, manifesting the electrostatic interactions do not mainly account for their noncovalent interactions; while both electrostatic attraction interaction and orbital interactions contribute to the weak noncovalent interactions of Cu-12BF. To sum up, orbital interactions are the main contributor to form strong secondary metal-ligand interactions in S-heterocycle-fused Cu(I) complexes.

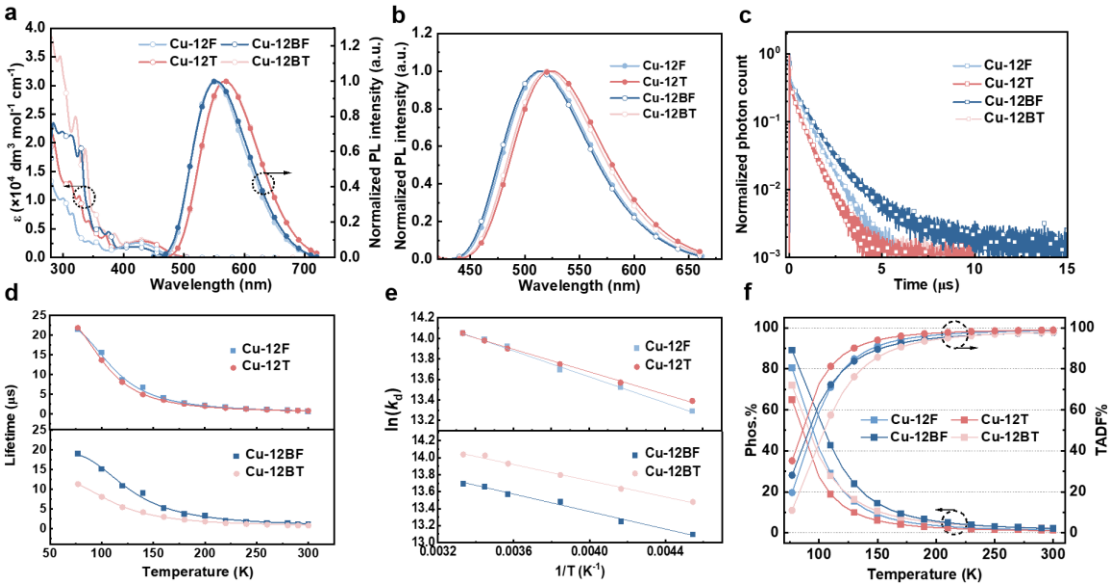

Figure 4. (a) UV-vis absorption and normalized fluorescence spectra of Cu-12F, Cu-12T, Cu-12BF, and Cu-12BT in toluene solutions (10^{-4} M, 300 K). (b) Normalized fluorescence spectra and (c) transient PL decay cruves of Cu-12F, Cu-12T, Cu-12BF, and Cu-12BT in mCBP-doped films with 5 wt% doping concentration. (d) Boltzmann-type and (e) Arrhenius-type fit to the temperature-dependent lifetime data (symbols) to **eq. S1-S4** (line) for the doped films of Cu-12F, Cu-12T, Cu-12BF, and Cu-12BT. (f) Temperature-dependent TADF and phosphorescence fractional intensities of Cu-12F, Cu-12T, Cu-12BF, and Cu-12BT.

TADF properties

As illustrated in **Figure 4a**, although the ligand-attributed absorption bands of these complexes were similar, the absorption peaks from ligand-ligand charge transfer (LLCT) transition followed the order of Cu-12BF (425 nm) ≈ Cu-12F (426 nm) < Cu-12BT (431 nm) ≈ Cu-12T (432 nm). Similarly, Cu-12F and Cu-12BF exhibited nearly identical PL profiles together with significant emission blue-shifts of 5~18 nm in solution and film state compared with those of Cu-12T and Cu-12BT, respectively. These results suggested the steady-state photophysics of these complexes largely depended on donor ligands. To clarify this point, density functional theory (DFT) and time-dependent DFT (TD-DFT) calculations were performed. As a result, the simulated

S_1 levels of these complexes were gradually declined as the decrease of donor ligand strength, that is Cu-12BF (2.46 eV, 504 nm) ≈ Cu-12F (2.42 eV, 513 nm) > Cu-12BT (2.29 eV, 541 nm) ≈ Cu-12T (2.25 eV, 550 nm). This calculated S_1 tendency was basically consistent with the order of PL emission peaks for these complexes (**Table 1**). These results pinpointed the excited state energies of these complexes are mainly determined by the electronic properties of donor ligands.

To get insight into exciton dynamics of these complexes, we conducted transient photoluminescence (PL) curves. All the complexes manifested double exponential decay profiles composed of ps-scale intersystem-crossing-dominant components (shown in **Figure S5a**) and μs-scale delayed fluorescence (DF) radiations in both solution and film states (**Figure 4c** and **S5b** and **Table 1**). In comparison with the S-embedded complexes, the DF lifetimes of the O-embedded complexes were slightly elongated. To further picture the exciton dynamics of these complexes, temperature-dependent lifetimes of these complexes were measured. As shown in **Figure 4d**, when cooling down to 77 K, all these complexes exhibited two orders of magnitude longer average decay lifetimes than those at 300 K, solidly establishing their TADF nature (**Figure S6** and **Table S5**). Fits of temperature-dependent emissive lifetimes to Boltzmann- and Arrhenius-type fittings were also performed (**Figure 4d**, **4f, S7** and **S8**). As listed in **Table 1**, the O-embedded complexes afforded slightly larger ΔE_{ST} of ~50 meV in comparison with those of the S-embedded complexes (~45 meV). This could be ascribed to the longer-range LLCT for Cu-12T and Cu-12BT, according to the hole-electron analysis of S_1 states (**Figure S9** and **S10**). Moreover, the slightly higher

phosphorescent proportion could be responsible for the longer exciton lifetime (1.13 μs) of Cu-12BF compared with those of other complexes (0.79-0.84 μs).

Subsequently, these complexes had significantly different Φ_{PL}s (**Table 1**), mainly depending on donor ligands. Cu-12T exhibited superior Φ_{PL} of 70% compared with that of Cu-12F (47%); whereas Cu-12BF and Cu-12BT possessed significantly enhanced Φ_{PL}s of 91% and 93%, respectively, comparable to the best values reported for Cu(I) complexes to date.[13,14] To figure out this point, the key photophysical rate constants were extracted. Accordingly, all the complexes exhibited similar k_r ranging from 0.56×10^6 to 1.16×10^6 s^{-1}. Differently, their nonradiative rate constants (k_{nr}) fell in the order of Cu-12F (0.63×10^6 s^{-1}) > Cu-12T (0.38×10^6 s^{-1}) > Cu-12BT (0.09×10^6 s^{-1}) ≈ Cu-12BF (0.08×10^6 s^{-1}), inversely related to the variation trend of Φ_{PL}. In this context, the Φ_{PL}s of these Cu(I) complexes could be mainly determined by the nonradiative processes, which are highly associated to the conformation dynamics.

Table 1. Photophysical properties in solution and film states.

compound	λ_{PL} [a)/b)] [nm]	Φ_{PL} [b)] [%]	τ_d [a)/b)] [μs]	k_r [c)] [10^6 s^{-1}]	k_{nr} [d)] [10^6 s^{-1}]	ΔE_{ST} [e)/f)] [meV]
Cu-12F	552/514	47	0.37/0.84	0.56	0.63	51/52
Cu-12T	569/525	70	0.29/0.79	0.89	0.38	46/48
Cu-12BF	551/516	91	0.39/1.13	0.81	0.08	53/47
Cu-12BT	569/521	93	0.37/0.80	1.16	0.09	42/43

a) Measured in diluted toluene solutions (10^{-4} M, 300 K). b) Measured in mCBP-doped films with doping concentration of 5 wt%. c) $k_r=\Phi_{PL}/\tau_d$. d) $k_{nr}=\Phi_{PL}(1/k_r-1)$. e) Fitted from two-level Boltzmann-type dynamic model. f) Fitted from Arrhenius-type dynamic model.

Conformation dynamics

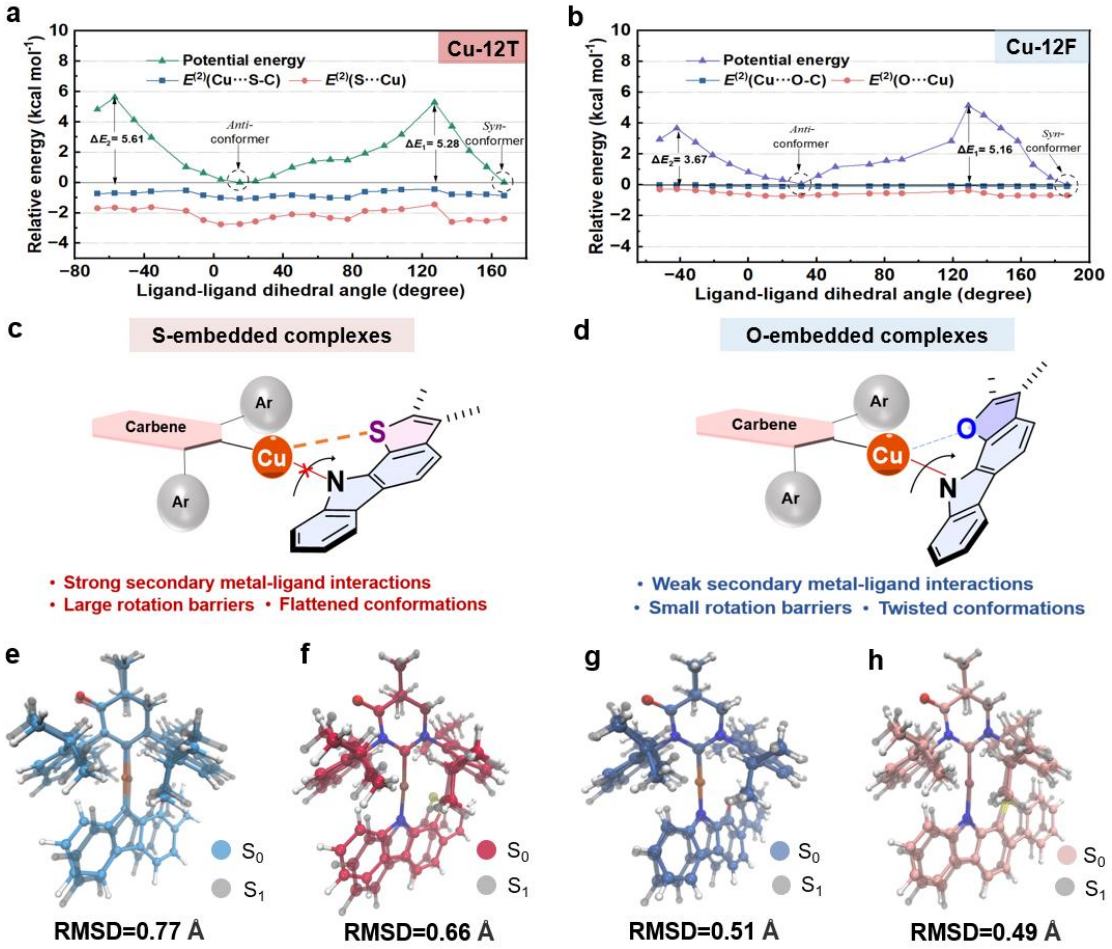

Figure 5. Evolution of potential energy and $E^{(2)}$ of noncovalent interactions of (a) Cu-12F and (b) Cu-12T. Schematic diagram of the correlation between molecular conformation and noncovalent interlocked interaction for the (c) O-embedded and (d) S-embedded complexes. Geometric deformation between the optimized S_0 and S_1 conformation of (e) Cu-12F, (f) Cu-12T, (g) Cu-12BF, and (h) Cu-12BT.

To understand the influence of conformation dynamics on the photophysical properties, we conducted the flexible potential energy surface scanning with respect to the ligand-ligand dihedral angle. As illustrated in **Figure 5a** and **5b**, the optimal *anti*-conformation of Cu-12T delivered smaller ligand-ligand dihedral angle (16^o) compared with that of Cu-12F (32^o), in accordance with the angles observed in single-crystal structures (**Figure 2**). The rotation energy barriers of Cu-12T were also slightly higher than those of Cu-12F. Similar tendency was observed for Cu-12BF and Cu-12BT

(**Figure S12**), yet their rotation barriers were much larger due to the sufficient steric hindrance between carbene flank and fused phenyl moiety on amide ligand. Intriguingly, the stabilization energy of secondary metal-ligand interactions of the O- and S-embedded complexes exhibited different evolving tendencies with respect to the ligand-ligand rotation. For the S-embedded complexes, S···Cu and Cu···S−C interactions gradually became weak as the conformation changed from coplanar to vertical, accompanied with the $E^{(2)}$ increment of ~1.5 and ~0.3 kcal mol^{-1}, respectively. Such a loss of stabilization energy induced by the ligand-ligand rotation is equivalent to ~30% of the rotation barrier for the S-embedded complexes (**Figure 5a** and **S12a**). In contrast, the $E^{(2)}$ of O···Cu and Cu···O−C interactions were kept small and basically independent of the conformation evolution (**Figure 5b** and **S12b**). In this sense, the strong secondary metal-ligand interactions in the S-embedded complexes afford sizable noncovalent stabilization energies and support larger ligand-ligand rotation barriers, ultimately flattening the ground state conformations (**Figure 5c**). Whereas, the weak secondary metal-ligand interactions have a small influence on the conformation dynamics of the O-embedded complexes and render twisted conformations (**Figure 5d**). Furthermore, the S-embedded complexes possessed smaller ligand-ligand twisted angles in S_1 states with respect to the O-embedded complexes (**Figure S13**). This suggests the strong secondary metal-ligand interactions can suppress ligand-ligand rotation in excited states to some extent. Subsequently, root mean square deviation (RMSD) between S_0 and S_1 in these complexes were calculated for the quantitative estimation of excited state reorganization. As displayed in **Figure 5e** and **5f**, Cu-12T delivered smaller

RMSD of 0.66 Å than that of Cu-12F (0.77 Å), which can be attributed to the stronger secondary metal-ligand interactions of Cu-12T. Differently, Cu-12BF and Cu-12BT were imparted with small and similar RMSD values (**Figure 5g** and **5h**), consistent with the high Φ_{PL}s of both complexes. This pinpoints the conformation dynamics and excited state reorganizations of Cu-12BF and Cu-12BT are mainly determined by steric hindrance between carbene and amide ligands. With the fusion of additional phenyl moiety on the amide ligands, the significantly enhanced steric hindrance gave rise to considerable ligand-ligand rotation barriers and thus confined the conformations. To sum up, in the coordination sphere with insufficient steric hindrance, strong secondary metal-ligand interactions can confine conformational deformation and suppress excited state reorganizations of two-coordinate Cu(I) complexes, thus supporting high Φ_{PL}s. Comparatively, for the Cu(I) complexes bearing sterically hindered subunits, secondary metal-ligand interactions can also serve as a complementary contributor to the conformation dynamics that are mainly controlled by steric hindrance effect.

Conclusion

In summary, we have developed a series of Cu(I)-based TADF complexes possessing CMA motif by using chalcogen-heterocycle-fused carbazole derivatives as donor ligands. Similar with typical CMA complexes, the emission wavelength and exciton lifetimes of these complexes are strongly associated with the electronic properties of primary-sphere ligands. Furthermore, specific secondary metal-ligand interactions existed between the central copper and chalcogen-heterocycle subunits. More

importantly, such unique interactions are beneficial to optimize conformation dynamics and limit excited state reorganization of Cu(I) CMA complexes. Combined with the steric hindrance effect, the S-embedded complexes realized high photoluminescence quantum yields of up to 93% along with high radiative rate constants of up to 1.2 $\times 10^6$ s^{-1}. This finding not only opens a new avenue for the development of efficient CMA complexes *via* noncovalent interactions, but also disclose the large potential of Cu(I) emitters in the OLED field.

Acknowledgements

S. G. gratefully acknowledges financial support from the National Natural Science Foundation of China (52022071). The numerical calculations in this paper have been done on the supercomputing system in the Supercomputing Center of Wuhan University. We thank Prof. Cheng Zhong (Wuhan University) for his helpful suggestions on theoretical calculations.

References

(1) (a) Zheng, Y. Q.; Lei, T.; Dou, J. H.; Xia, X.; Wang, J. Y.; Liu, C. J.; Pei, J., Strong Electron-Deficient Polymers Lead to High Electron Mobility in Air and Their Morphology-Dependent Transport Behaviors. *Adv. Mater.* **2016**, *28*, 7213-7219; (b) Huang, H.; Yang, L.; Facchetti, A.; Marks, T. J., Organic and Polymeric Semiconductors Enhanced by Noncovalent Conformational Locks. *Chem. Rev*. **2017**,

117, 10291-10318; (c) Liu, B.; Rocca, D.; Yan, H.; Pan, D., Beyond Conformational Control: Effects of Noncovalent Interactions on Molecular Electronic Properties of Conjugated Polymers. *JACS Au* **2021**, *1*, 2182-2187; (d) Peng, Q.; Ma, H.; Shuai, Z., Theory of Long-Lived Room-Temperature Phosphorescence in Organic Aggregates. *Acc. Chem. Res.* **2021**, *54*, 940-949; (e) Zhu, C.; Luo, Q.; Shen, Y.; Lv, C.; Zhao, S.; Lv, X.; Cao, F.; Wang, K.; Song, Q.; Zhang, C.; Zhang, Y., Red to Near-Infrared Mechanochromism from Metal-free Polycrystals: Noncovalent Conformational Locks Facilitating Wide-Range Redshift. *Angew. Chem. Int. Ed.* **2021**, *60*, 8510-8514.

(2) (a) Liu, Y.; Zhang, Z.; Feng, S.; Li, M.; Wu, L.; Hou, R.; Xu, X.; Chen, X.; Bo, Z., Exploiting Noncovalently Conformational Locking as a Design Strategy for High Performance Fused-Ring Electron Acceptor Used in Polymer Solar Cells. *J. Am. Chem. Soc.* **2017**, *139*, 3356-3359; (b) Liu, Y.; Song, J.; Bo, Z., Designing High Performance Conjugated Materials for Photovoltaic Cells with the Aid of Intramolecular Noncovalent Interactions. *Chem. Commun.* **2021**, *57*, 302-314; (c) Gu, X.; Wei, Y. Liu, X.; Yu, N.; Li, L.; Han, Z.; Gao, J.; Li, C.; Wei, Z.; Tang, Z.; Zhang, X.; Huang, H., Low-Cost Polymer Acceptors with Noncovalently Fused-Ring Backbones for Efficient All-Polymer Solar Cells. *Sci. China Chem.* **2022**, *65*, 926-933.

(3) (a) Di, C.-A.; Zhang, F.; Zhu, D., Multi-Functional Integration of Organic Field-Effect Transistors (OFETs): Advances and Perspectives. *Adv. Mater.* **2013**, *25*, 313-330; (b) Chen, Z.; Li, M.; Hu, M.; Wang, S.; Miao, Z.; Xu, S.; Chen, C.; Dong, H.; Huang, W.; Chen, R., All-Acceptor Polymers with Noncovalent Interactions for Efficient Ambipolar Transistors. *J. Mater. Chem. C* **2020**, *8*, 2094-2101; (c) Li, H.; Shi, Y.; Han,

G.; Liu, J.; Zhang, J.; Li, C.; Liu, J.; Yi, Y.; Li, T.; Gao, X.; Di, C.; Huang, J.; Che, Y.; Wang, D.; Hu, W.; Liu, Y.; Jiang, L., Monolayer Two-Dimensional Molecular Crystals for an Ultrasensitive OFET-based Chemical Sensor. *Angew. Chem. Int. Ed.* **2020**, *59*, 4380-4384.

(4) (a) Rajamalli, P.; Senthilkumar, N.; Gandeepan, P.; Huang, P.-Y.; Huang, M.-J.; Ren-Wu, C.-Z.; Yang, C.-Y.; Chiu, M.-J.; Chu, L.-K.; Lin, H.-W.; Cheng, C.-H., A New Molecular Design Based on Thermally Activated Delayed Fluorescence for Highly Efficient Organic Light Emitting Diodes. *J. Am. Chem. Soc.* **2016**, *138*, 628-634; (b) Chen, X.-K.; Bakr, B. W.; Auffray, M.; Tsuchiya, Y.; Sherrill, C. D.; Adachi, C.; Bredas, J.-L., Intramolecular Noncovalent Interactions Facilitate Thermally Activated Delayed Fluorescence (TADF). *J. Phys. Chem. Lett.* **2019**, *10*, 3260-3268; (c) Xue, J.; Liang, Q. Wang, R.; Hou, J.; Li, W.; Peng, Q.; Shuai, Z.; Qiao, J., Highly Efficient Thermally Activated Delayed Fluorescence via J-Aggregates with Strong Intermolecular Charge Transfer. *Adv. Mater.* **2019**, *31*, e1808242.

(5) (a) Yang, J.; Zhen, X.; Wang, B.; Gao, X.; Ren, Z.; Wang, J.; Xie, Y.; Li, J.; Peng, Q.; Pu, K.; Li, Z., The Influence of the Molecular Packing on the Room Temperature Phosphorescence of Purely Organic Luminogens. *Nat. Commun.* **2018**, *9*, 840; (b) Wang, W.; Zhang, Y.; Jin, W. J., Halogen Bonding in Room-Temperature Phosphorescent Materials. *Coordin. Chem. Rev.* **2020**, *404*, 213107; (c) Wu, H.; Wang, D.; Zhao, Z.; Wang, D.; Xiong, Y.; Tang, B. Z., Tailoring Noncovalent Interactions to Activate Persistent Room-Temperature Phosphorescence from Doped Polyacrylonitrile Films. *Adv. Funct. Mater.* **2021**, *31*, 2101656; (d) Sun, M. J.; Anhalt, O.; Sarosi, M. B.;

Stolte, M.; Wurthner, F., Activating Organic Phosphorescence via Heavy Metal-π Interaction Induced Intersystem Crossing. *Adv. Mater.* **2022**, *34*, e2207331.

(6) (a) Shook, R. L.; Borovik, A. S., Role of the Secondary Coordination Sphere in Metal-Mediated Dioxygen Activation. *Inorg. Chem.* **2010**, *49*, 3646-3660; (b) Raynal, M.; Ballester, P.; Vidal-Ferran, A.; van Leeuwen, P. W., Supramolecular Catalysis. Part 1: Non-covalent Interactions as a Tool for Building and Modifying Homogeneous Catalysts. *Chem. Soc. Rev.* **2014**, *43*, 1660-1733; (c) Drover, M. W., A Guide to Secondary Coordination Sphere Editing. *Chem. Soc. Rev.* **2022**, *51*, 1861-1880.

(7) (a) Brown, C. J.; Toste, F. D.; Bergman, R. G.; Raymond, K. N., Supramolecular Catalysis in Metal-Ligand Cluster Hosts. *Chem. Rev.* **2015**, *115*, 3012-3035; (b) Wei, P.; Yan, X.; Huang, F., Supramolecular Polymers Constructed by Orthogonal Self-Assembly Based on Host-Guest and Metal-Ligand Interactions. *Chem. Soc. Rev.* **2015**, *44*, 815-832.

(8) (a) Bizzarri, C.; Spuling, E.; Knoll, D. M.; Volz, D.; Brase, S., Sustainable Metal Complexes for Organic Light-Emitting diodes (OLEDs). *Coordin. Chem. Rev.* **2018**, *373*, 49-82; (b) Liu, Y.; Yiu, S.-C.; Ho, C.-L.; Wong, W.-Y., Recent Advances in Copper Complexes for Electrical/Light Energy Conversion. *Coordin. Chem. Rev.* **2018**, *375*, 514-557.

(9) McMillin, D. R.; Buckner, M. T.; Ahn, B. T. *Inorg. Chem.* **1977**, *16*, 943-945.

(10) (a) Hashimoto, M.; Igawa, S.; Yashima, M.; Kawata, I.; Hoshino, M.; Osawa, M., Highly Efficient Green Organic Light-Emitting Diodes Containing Luminescent Three-Coordinate Copper(I) Complexes. *J. Am. Chem. Soc.* **2011**, *133*, 10348-10351; (b)

Hashimoto, M.; Igawa, S.; Yashima, M.; Kawata, I.; Hoshino, M.; Osawa, M., Highly Efficient Green Organic Light-Emitting Diodes Containing Luminescent Three-Coordinate Copper(I) Complexes. *J. Am. Chem. Soc.* **2011**, *133*, 10348-103851; (c) Osawa, M.; Hoshino, M.; Hashimoto, M.; Kawata, I.; Igawa, S.; Yashima, M., Application of Three-Coordinate Copper(I) Complexes with Halide Ligands in Organic Light-Emitting Diodes that Exhibit Delayed Fluorescence. *Dalton Trans.* **2015**, *44*, 8369-8378; (d) Ma, X.-H.; Li, J.; Luo, P.; Hu, J.-H.; Han, Z.; Dong, X.-Y.; Xie, G.; Zang, S.-Q., Carbene-Stabilized Enantiopure Heterometallic Clusters Featuring EQE of 20.8% in Circularly-Polarized OLED. *Nat. Commun.* **2023**, *14*, 4121.

(11) (a) Igawa, S.; Hashimoto, M.; Kawata, I.; Yashima, M.; Hoshino, M.; Osawa, M., Highly Efficient Green Organic Light-Emitting Diodes Containing Luminescent Tetrahedral Copper(i) Complexes. *J. Mater. Chem. C* **2013**, *1*, 542-551; (b) Liu, Z.; Qiu, J.; Wei, F.; Wang, J.; Liu, X.; Helander, M. G.; Rodney, S.; Wang, Z.; Bian, Z.; Lu, Z.; Thompson, M. E.; Huang, C., Simple and High Efficiency Phosphorescence Organic Light-Emitting Diodes with Codeposited Copper(I) Emitter. *Chem. Mater.* **2014**, *26*, 2368-2373.

(12) (a) Lotito, K. J.; Peters, J. C., Efficient Luminescence from Easily Prepared Three-Coordinate Copper(I) Arylamidophosphines. *Chem. Commun.* **2010**, *46*, 3690-3692; (b) Muthig, A. M. T.; Mrózek, O.; Ferschke, T.; Rödel, M.; Ewald, B.; Kuhnt, J.; Lenczyk, C.; Pflaum, J.; Steffen, A., Mechano-Stimulus and Environment-Dependent Circularly Polarized TADF in Chiral Copper(I) Complexes and Their Application in OLEDs. *J. Am. Chem. Soc.* **2023**, *145*, 4438-4449.

(13) (a) Di, D.; Romanov, A. S.; Yang, L.; Richter, J. M.; Rivett, J. P. H.; Jones, S.; Thomas, T. H.; Abdi Jalebi, M.; Friend, R. H.; Linnolahti, M.; Bochmann, M.; Credgington, D. High-Performance Light Emitting Diodes Based on Carbene-Metal-Amides. *Science* **2017**, *356*, 159-163; (b) Hamze, R.; Peltier, J. L.; Sylvinson, D.; Jung, M.; Cardenas, J.; Haiges, R.; Soleilhavoup, M.; Jazzar, R.; Djurovich, P. I.; Bertrand, G.; Thompson, M. E. Eliminating Nonradiative Decay in Cu(I) Emitters: >99% Quantum Efficiency and Microsecond Lifetime. *Science* **2019**, *363*, 601-606; (c) Shi, S.; Jung, M. C.; Coburn, C.; Tadle, A.; Sylvinson, M. R. D.; Djurovich, P. I.; Forrest, S. R.; Thompson, M. E., Highly Efficient Photo- and Electroluminescence from Two-Coordinate Cu(I) Complexes Featuring Nonconventional *N*-Heterocyclic Carbenes. *J. Am. Chem. Soc.* **2019**, *141*, 3576-3588; (d) Gernert, M.; Balles-Wolf, L.; Kerner, F.; Muller, U.; Schmiedel, A.; Holzapfel, M Marian, C. M.; Pflaum, J.; Lambert, C.; Steffen, A., Cyclic (Amino)(aryl)carbenes Enter the Field of Chromophore Ligands: Expanded π System Leads to Unusually Deep Red Emitting Cu(I) Compounds. *J. Am. Chem. Soc.* **2020**, *142*, 8897-8909; (e) Muniz, C. N.; Schaab, J.; Razgoniaev, A.; Djurovich, P. I.; Thompson, M. E., π-Extended Ligands in Two-Coordinate Coinage Metal Complexes. *J. Am. Chem. Soc.* **2022**, *144*, 17916-17928; (f) Ying, A.; Gong, S., A Rising Star: Luminescent Carbene-Metal-Amide Complexes. *Chem. Eur. J.* **2023**, e202301885.

(14) (a) Ying, A.; Huang, Y.-H.; Lu, C.-H.; Chen, Z.; Lee, W.-K.; Zeng, X.; Chen, T.; Cao, X.; Wu, C.-C.; Gong, S.; Yang, C., High-Efficiency Red Electroluminescence Based on a Carbene-Cu(I)-Acridine Complex. *ACS Appl. Mater. Interfaces* **2021**, *13*,

13478-13486; (b) Gu, Q.; Chotard, F.; Eng, J.; Reponen, A. M.; Vitorica-Yrezabal, I. J.; Woodward, A. W.; Penfold, T. J.; Credgington, D.; Bochmann, M.; Romanov, A. S., Excited-State Lifetime Modulation by Twisted and Tilted Molecular Design in Carbene-Metal-Amide Photoemitters. *Chem. Mater.* **2022**, *34*, 7526-7542; (c) Tang, R.; Xu, S.; Lam, T.-L.; Cheng, G.; Du, L.; Wan, Q.; Yang, J.; Hung, F.-F.; Low, K.-H.; Phillips, D. L.; Che, C.-M., Highly Robust Cu^{I}-TADF Emitters for Vacuum-Deposited OLEDs with Luminance up to 222 200 cd m^{-2} and Device Lifetimes LT_{90} up to 1300 hours at an Initial Luminance of 1000 cd m^{-2}. *Angew. Chem. Int. Ed.* **2022**, *61*, e202203982. (d) Wang, H.-J.; Liu, Y.; Yu, B.; Song, S.-Q.; Zheng, Y.-X.; Liu, K.; Chen, P.; Wang, H.; Jiang, J.; Li, T.-Y., A Configurationally Confined Thermally Activated Delayed Fluorescent Two-Coordinate Cu^{I} Complex for Efficient Blue Electroluminescence. *Angew. Chem. Int. Ed.* **2022**, *62*, e202217195.

(15) (a) Romanov, A. S.; Jones, S. T. E.; Gu, Q.; Conaghan, P. J.; Drummond, B. H.; Feng, J.; Chotard, F.; Buizza, L.; Foley, M.; Linnolahti, M.; Credgington, D.; Bochmann, M., Carbene Metal Amide Photoemitters: Tailoring Conformationally Flexible Amides for Full Color Range Emissions Including White-Emitting OLED. *Chem. Sci.* **2020**, *11*, 435-446; (b) Ying, A.; Ai, Y.; Yang, C.; Gong, S., Aggregation-Dependent Circularly Polarized Luminescence and Thermally Activated Delayed Fluorescence from Chiral Carbene-Cu^{I}-Amide Enantiomers. *Angew. Chem. Int. Ed.* **2022**, *61*, e202210490.

(16) Mahmudov, K. T.; Gurbanov, A. V.; Aliyeva, V. A.; Guedes da Silva, M. F. C.; Resnati, G.; Pombeiro, A. J. L., Chalcogen Bonding in Coordination Chemistry. *Coordin. Chem. Rev.* **2022**, *464*, 214556.

(17) Campeau, L.-C.; Parisien, M.; Jean, A.; Fagnou, K., Catalytic Direct Arylation with Aryl Chlorides, Bromides, and Iodides: Intramolecular Studies Leading to New Intermolecular Reactions. *J. Am. Chem. Soc.* **2006**, *128*, 581-590.

(18) Hamze, R.; Shi, S.; Kapper, S. C.; Muthiah Ravinson, D. S.; Estergreen, L. Jung, M. C.; Tadle, A. C.; Haiges, R.; Djurovich, P. I.; Peltier, J. L.; Jazzar, R.; Bertrand, G.; Bradforth, S. E.; Thompson, M. E., "Quick-Silver" from a Systematic Study of Highly Luminescent, Two-Coordinate, d^{10} Coinage Metal Complexes. *J. Am. Chem. Soc.* **2019,** *141*, 8616-8626.

(19) (a) Lu, T.; Chen, F., Multiwfn: a multifunctional wavefunction analyzer. *J. Comput. Chem.* **2012**, *33*, 580-592; (b) Lefebvre, C.; Rubez, G.; Khartabil, H.; Boisson, J. C.; Contreras-Garcia, J.; Henon, E., Accurately Extracting the Signature of Intermolecular Interactions Present in the NCI Plot of the Reduced Density Gradient versus Electron Density. *Phys. Chem. Chem. Phys.* **2017**, *19*, 17928-17936.

(20) (a) Pascoe, D. J.; Ling, K. B.; Cockroft, S. L., The Origin of Chalcogen-Bonding Interactions. *J. Am. Chem. Soc.* **2017**, *139*, 15160-15167. (b) Liu, M.; Han, X.; Chen, H.; Peng, Q.; Huang, H., A Molecular Descriptor of Intramolecular Noncovalent Interaction for Regulating Optoelectronic Properties of Organic Semiconductors. *Nat. Commun.* **2023**, *14*, 2500.